Available online at www.sciencedirect.com
SCIENCE DIRECT®
Journal of Nuclear Materials 323 (2003) 268–280
journal of nuclear materials
www.elsevier.com/locate/jnucmat

Void and precipitate strengthening in α-iron: what can we learn from atomic-level modelling?

Yu.N. Osetsky *, D.J. Bacon

Department of Engineering, The University of Liverpool, Brownlow Hill L69 3GH, Liverpool, UK

Abstract

Defects created by radiation damage in materials can form obstacles to dislocation glide and thereby change the mechanical properties. Development of models of these effects requires understanding of the phenomena involved at both the atomic and continuum levels. This paper concentrates on the former level, and describes the application of a model developed recently to study the motion of an initially straight edge dislocation through a row of either voids or coherent copper precipitates in α-iron. The model can provide quantitative information on the stress–strain relationship, energy barrier profile and strength characteristics for dislocation–obstacle interaction, and the effects of stress, strain rate and temperature on the process can be investigated. New results on data and atomic-scale mechanisms associated with strengthening due to voids and precipitates over a range of size are presented and compared with earlier continuum treatments. It is shown that atomic-level simulation is essential for revealing information required for multiscale modelling of phenomena in radiation damage.

PACS: 31.15.Qg; 61.72.Bb; 61.72.Lk

1. Introduction

Defects formed by radiation damage in metals are responsible for significant changes in mechanical properties, including yield stress, work hardening rate and ductility. Understanding the mechanisms of such changes is necessary for creation of predictive models for estimation of lifetime of power plant components. In order to achieve this, much effort is currently being focused on multiscale materials modelling. This involves the coupling of different theoretical and computational techniques, each with its own range of applicability for the length and time scales of the phenomena under consideration. It is necessary for information gained from fine-scale calculations to provide data and mechanisms for coarser-scale models. An important issue of this approach is the coupling between the levels, since this can be made only via overlapping scales of the particular techniques. One of the most important interfaces in the area of radiation damage and mechanical properties lies between the atomic and continuum scales. Elasticity theory of dislocations provides a valid description of the role of dislocations in the mechanical response of materials, but there are problems in treating within continuum theory processes that are controlled by atomic-scale mechanisms. One of the most important examples is the interaction of dislocations with obstacles to their glide. With current computing power, many such phenomena can now be studied by atomic modelling techniques, and the important question of how the atomic and continuum approaches can be mutually validated within the same scale can be tackled.

We have recently developed a model to investigate the behaviour at the atomic scale of a dislocation gliding in a crystal with or without obstacles [1]. It is a development of an approach [2] based on a periodic array of dislocations (PAD), in which the model crystal contains

* Corresponding author. Address: Computer Sciences and Mathematics Division, Oak Ridge National Laboratory, Bldg. 4500S, MS-6138, P.O. Box 2008, Oak Ridge, TN 37831-6158, USA. Tel.: +1-865 576 3254; fax: +1-856 241 3650.
E-mail address: yri@ornl.gov (Yu.N. Osetsky).

0022-3115/$ - see front matter © 2003 Elsevier B.V. All rights reserved.
doi:10.1016/j.jnucmat.2003.08.028

an initially straight *edge* dislocation and periodic boundary conditions are applied not only along the dislocation line but also the direction of the Burgers vector $\boldsymbol{b}$. This allows the possibility of moving a dislocation over long distances with independent application of external effects such as applied stress or strain. The resultant response such as strain (elastic and plastic) or stress and crystal energy may be calculated with realistic dislocation density and spacing between obstacles. Simulation may be carried out for either zero or non-zero temperature, T.

The model has been applied initially to α-iron. Examples of relevant extended crystal defects that can interact with a gliding dislocation in iron and ferritic alloys include dislocation loops, voids and secondary phase precipitates: among the latter, precipitates of copper in pressure vessel steels are particularly important. Initial results on the interaction between an initially straight edge dislocation and either voids or coherent copper precipitates in iron at zero temperature are presented elsewhere [3]. Here, we review and extend them for non-zero temperature and, by comparing with previous studies based on the continuum approximation, draw conclusions on the importance of treating the problem at atomic scale.

2. Model

The modelling method is described in detail in [1]. In summary, to simulate an infinitely long, straight edge dislocation lying parallel to the z-axis with the Burgers vector $\boldsymbol{b}$ along the x-axis, the following procedure is adopted. Two half-crystals strained to have different lattice parameters in the direction **b** are joined along the dislocation slip plane $y = 0$. The upper and lower half-crystals have N and $N - 1$ $y - z$ lattice planes, respectively, so that after relaxation the edge dislocation is created in the centre (Note that the dislocation thus formed is *not* a 'misfit dislocation' but a crystal Volterra dislocation [1].). The simulated crystal is sketched in Fig. 1, where the edge dislocation is one of minimum energy with Burgers vector $1/2[1\,1\,1]$ in a bcc lattice. The slip plane is $(1\,\bar{1}\,0)$ and the line direction is $[1\,1\,\bar{2}]$. The inner region, A, of mobile atoms has x, y and z dimensions L_b, H and L, respectively. Periodic boundary conditions are applied along x and z. Regions P of thickness of R_{cut}, where R_{cut} is the effective range of the interatomic potential, represent part of image crystallites whose atoms interact with those from region A. The regions B and F represent blocks of 'perfect' crystal where individual atoms are immobile. These rigid blocks are also subject to periodic replication along the x and z directions. For simplicity the block F is fixed and shear stress or strain is applied via force on, or displacement of, block B.

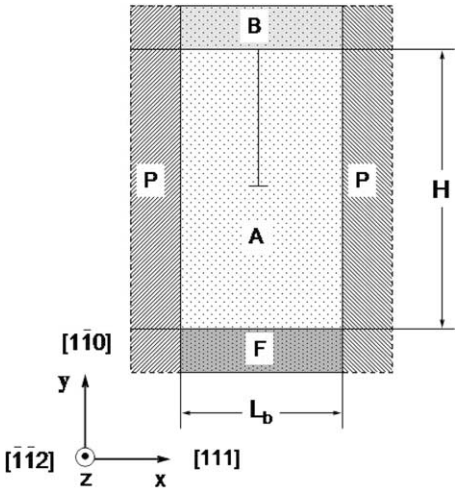

Fig. 1. Schematic presentation of simulated crystallite: A – region of mobile atoms; P – regions where periodic boundaries are applied; F – lower fixed block and B – upper rigid mobile block (from [1]).

The obstacle, consisting of either a void of vacancies or a coherent bcc precipitate of copper atoms, was as near spherical, diameter D, as possible with the equator coinciding with the glide plane $y = 0$ of the dislocation. The periodic boundary conditions along z result in a periodic array of obstacles of spacing L. Two qualitatively different techniques were used to simulate the dislocation overcoming these obstacles, as follows:

1. Using static relaxation ($T = 0$ K), shear deformation was introduced by the incremental displacement of block B in the x direction. At each step, the crystal was relaxed to minimise the potential energy and the applied shear stress was calculated as

$$\sigma_{xy} = F_{\mathrm{Int}}/A_{xz}, \tag{1}$$

where F_{Int} is the x component of the total force from all atoms in A on block B and A_{xz} is area of the x–z cross-section of the crystallite of mobile atoms A. The applied shear strain was increased incrementally until the dislocation overcame the obstacle row. A relatively small strain increment $\Delta\varepsilon = 10^{-4}$ was found to reproduce the stress–strain dependence with an inaccuracy in stress of <10 MPa. This set of simulations is both interesting and important because, with dynamic and thermal effects being absent, the results should be directly comparable with those obtained from continuum models (see Section 5).
2. In molecular dynamics (MD) simulation ($T > 0$ K), applied shear stress, τ, or strain rate, $\dot{\varepsilon}$, was applied. τ was introduced via a force along x applied to the centre of mass of B, which was treated as a particle

whose equations of motion were coupled with those of all mobile atoms. The effective mass of B is a parameter which can mimic rest of the crystal in investigation of kinetic effects in dislocation–obstacle interaction. $\dot{\varepsilon}$ was imposed by moving B along x at a desired rate, with the generated stress estimated using (1) averaged over 100–200 time steps (time step $t_s \approx 10^{-15}$ s).

In both the $T = 0$ and applied $\dot{\varepsilon}$ ($T > 0$) schemes, the maximum value of τ was taken as the critical resolved shear stress (CRSS), τ_c, for the dislocation to move through the array of obstacles. The atomic structure of the obstacle and dislocation was analysed at each step of strain increment in static modelling and every 100 time steps in MD. Identification and visualisation of the location of the core of the dislocation line is important, and the method used is described in [1].

In extending the simulations presented in [3], we have considered obstacles of diameter from 0.9 to 4.0 nm and containing from 27 to 2904 vacancies or Cu atoms. Four crystal sizes have now been used, all with $H = 19.9$ nm ($\approx 80b$). Crystal C1 had $L_b = 29.8$ nm ($= 120b$) and $L = 41.4$ nm ($\approx 167b$), C2 had $L_b = 59.6$ nm ($= 240b$) and $L = 41.4$ nm, C3 had $L_b = 120b$ and $L = 83$ nm ($\approx 334b$) and C4 had $L = 61.8$ nm and $L_b = 59.6$ nm ($= 240b$). C1 contained about 2 000 000 mobile atoms; C2 and C3 about 4 000 000 and C4 about 6 000 000. C1 and C2 were chosen to test the dependence of results on distance, L_b, between dislocations of the periodic array, C1 and C3 to test the effect of obstacle spacing, L, and C4 allows the dependence of the strengthening effect on both L and L_b to be tested. Finnis–Sinclair type many-body potentials derived by Ackland et al. [4,5] for the Fe–Cu binary system were used for all simulations.

3. Results for dislocation–void interaction

3.1. Dislocation–void interaction at $T = 0$ K

Fig. 2 shows results for 339 vacancy (diameter 2 nm) voids in models C1, C2 and C3 from [1] for shear stress and change in crystal potential energy, ΔE, as strain is increased incrementally from zero, starting from the initial unstrained state when the straight dislocation does not interact with the voids. The four regions I–IV correspond to I: dislocation glide in an otherwise perfect crystal; II: dislocation–void intersection, when the length of the dislocation is reduced but a step of width b is created on the entry surface of the void; III: dislocation bowing between the voids under the increasing applied strain; and IV: dislocation release from the void, leaving a step on the exit surface, i.e. the void is sheared. Furthermore, on breaking away from a void, the dislocation absorbs a few vacancies, thereby creating a superjog on the dislocation line. The contributions to ΔE are discussed in [1] and [3]: here we focus on τ.

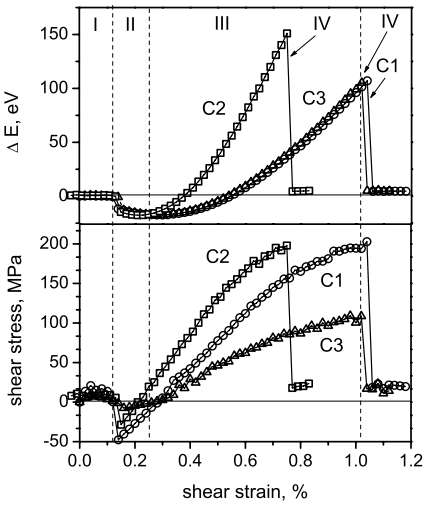

Fig. 2. Strain energy and applied stress as function of applied strain in crystal models C1, C2 and C3 containing an edge dislocation gliding through a row of voids, each having a diameter of 2 nm and containing 339 vacancies at $T = 0$ K.

The configuration of the dislocation just before it leaves the void in model C1 is presented as line C1 in Fig. 3(a). Line C3 in the equivalent figure for crystal C3, where the void-void spacing, L, is doubled. The two lines are similar in shape in the vicinity of the void, although away from it the line in C3 bows out further, as shown in Fig. 3(b). In both cases, the dislocation core energy leads to a preference for segments lying along low index directions, of which [1 1 1] is the orientation of screw segments as the dislocation leaves the void. The critical resolved shear stress τ_c is 207 MPa for C1 and 108 MPa for C3, the ratio of which is $\sim$1.9 and close to the reciprocal of the ratio of void spacing. This inverse dependence on L is as predicted by elasticity theory of dislocations for strengthening by localised obstacles (e.g. Chapter 10 of Hull and Bacon [6]). The CRSS and line shape have been determined over a range of D and L values. Earlier results [3] for $L = 41.4$ nm (C1 and C2) and for $L = 83$ nm (C3) have now been added to by simulations for $L = 61.8$ nm (C4) and the complete set of results for τ_c versus of void diameter (log scale) are presented in Fig. 4. All these plots are close to linear, with gradient in the ratios 1.9:1.3:1.0 for (C1, C2):C4:C3, which are close to the reciprocal of the ratios of the respective L values 2.0:1.3:1.0.

It is shown in [3] that the mechanism of dislocation–void interaction is void-size dependent. For small voids ($D < 2$ nm), the angle, φ, between dislocation segments as they emerge from a void at τ_c decreases with increasing D, becoming close to zero for $D = 2$ nm (see

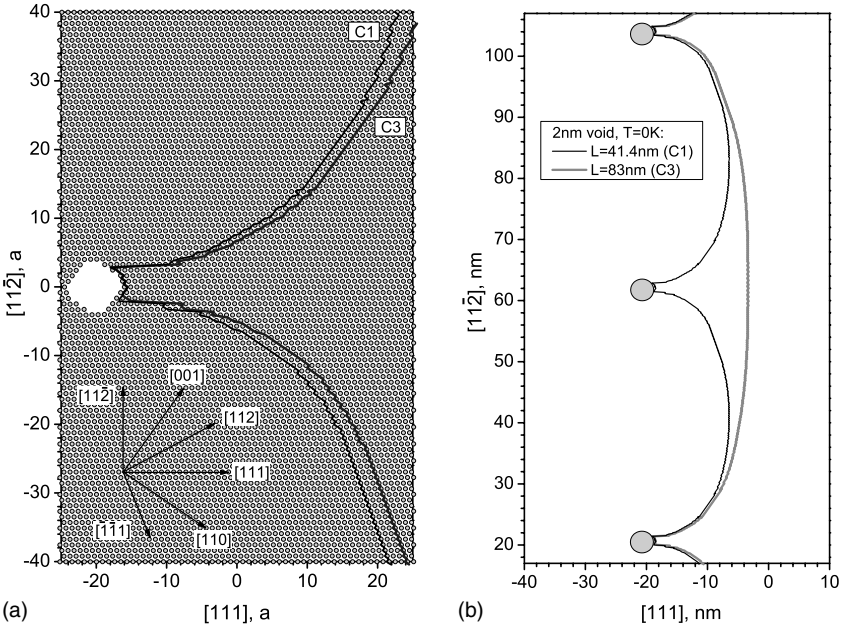

Fig. 3. Position of (a) atoms and (a, b) dislocation lines in [1 $\bar{1}$ 0] projection through the 2 nm void equator (coincident with the dislocation glide plane) in crystals C1 and C3 at the critical stress (from [3]).

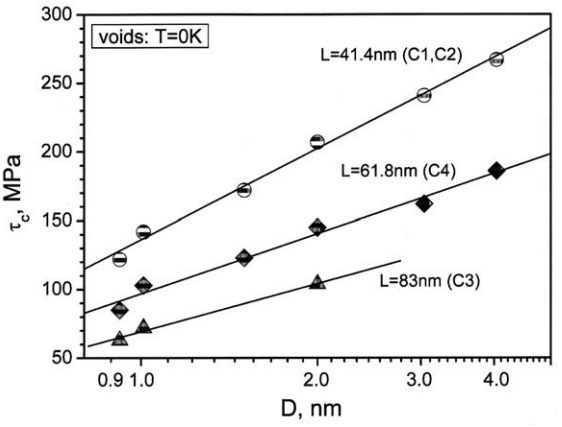

Fig. 4. Dependence of the value of critical resolved shear stress, τ_c, at $T = 0$ K against void diameter: circles are for models C1 and C2, diamonds for C4 and triangles for C3.

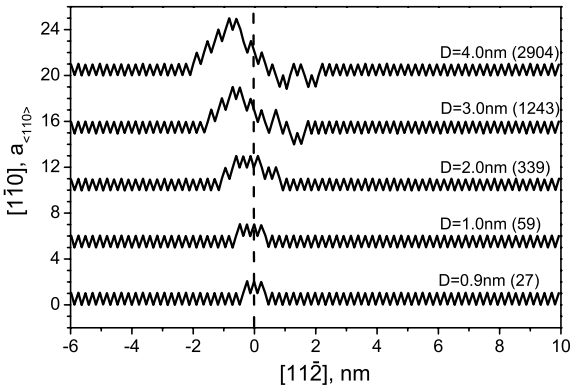

Fig. 5. Dislocation line viewed in [1 1 1] projection perpendicular to ***b*** after intersecting voids of different size D (and number of vacancies), at $T = 0$ K [3].

Fig. 3) and remaining zero for larger voids. This critical angle is similar to that expected for the Orowan mechanism, although creation of an Orowan loop does not occur around the void. Further increase of τ_c for larger voids is reflected only in the increase of the length and spacing of the two parallel screw segments of opposite sign that emerge from the void. The line breakaway mechanism is also complicated by climb, for the dislocation absorbs some vacancies as it breaks from the void, i.e. void size decreases due to interaction with the dislocation. The shape of a dislocation in [1 1 1] projection after it is released from voids of different size is presented in Fig. 5. The number vacancies removed from voids of diameter from 0.9 to 4 nm (27–2904 vacancies) varies from 5 to 19 respectively. The result of this effect on the form of the surface step created at the void by the dislocation is presented in Fig. 6 of [3].

3.2. dislocation–void interaction at $T > 0$ K

Stress–strain dependences obtained from modelling a 2 nm void in the C1 crystal at 100 K with different

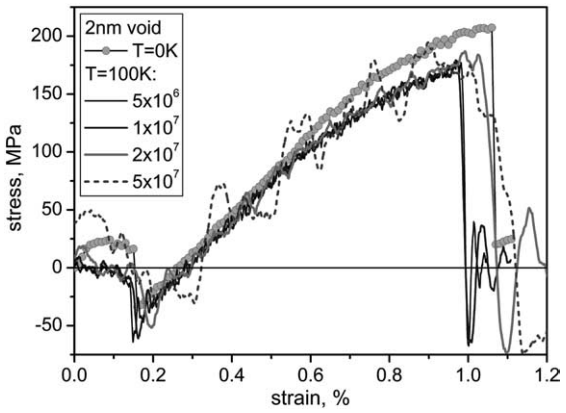

Fig. 6. Applied stress as function of strain in crystal C1 containing a dislocation gliding through a row of 2 nm voids. Circles are for the static simulation ($T = 0$ K) and lines are for different constant strain rates applied at $T = 100$ K, as indicated.

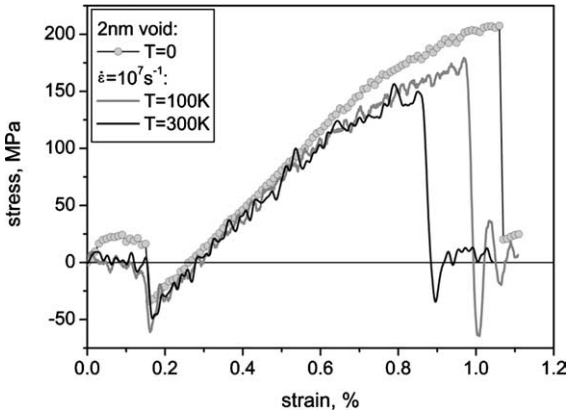

Fig. 7. Applied stress as function of strain in crystal C1 with 2 nm void at different temperatures. Data for 100 and 300 K were obtained at $\dot{\varepsilon} = 10^7$ s^{-1}.

constant applied strain rates, $\dot{\varepsilon}$, are presented in Fig. 6, where the static ($T = 0$ K) plot from Fig. 2 is included for comparison. It can be seen that although the fluctuations in stress are significant at $\dot{\varepsilon} > 10^7$ s^{-1} the maximum stress at 100K is lower than that at $T = 0$ K. It may be noted that for the crystal C1, strain rate effects become negligible at $\dot{\varepsilon} \leqslant 10^7$ s^{-1}, for the minimum modelled, $\dot{\varepsilon} = 2 \times 10^6$ s^{-1}, generated a stress–strain dependence similar to those at 5×10^6 s^{-1} and 10^7 s^{-1}. This demonstrates that modelling a dislocation moving with velocity $V_d \leqslant 60$ m/s, which is shown in [1] to correspond to the case $\dot{\varepsilon} = 10^7$ s^{-1} for C1, allows τ_c to be obtained with good accuracy. It may also be noted that this limit depends on crystal size, because the velocity of the dislocation in a PAD obeys the classical Orowan relation between V_d, $\dot{\varepsilon}$ and dislocation density $(L_b H)^{-1}$ (see [1]). The critical stress is temperature dependent, as can be seen in Fig. 7 where stress–strain dependences at $T = 0$, 100 and 300 K are presented. (The $T = 0$ K plot is taken from static modelling (Fig. 2) whereas those for $T = 100$ and 300 K were obtained with $\dot{\varepsilon} = 10^7$ s^{-1}.) The value of τ_c at 300 K is about 75% of that at 0 K and there is a significant decrease in the corresponding critical strain. Temperature also affects the shape of the dislocation line at the critical stress. This can be seen in Fig. 8 where the dislocation line just before it breaks from the 2 nm void in the static case (as in Fig. 3(a)) is compared with that for $\dot{\varepsilon} = 10^7$ s^{-1} at 300 K. The dislocation line bows out less and has a significantly larger breaking angle at 300 K than that at 0 K. Overall, the outcome of dislocation–void interaction at non-zero temperature is similar to that at $T = 0$ K, i.e. voids are sheared and dislocations become jogged.

Simulation of dislocation–void interaction under applied shear stress at $T > 0$ K shows that the outcome

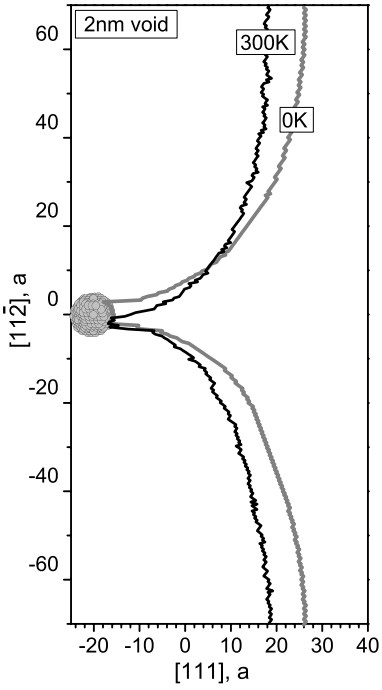

Fig. 8. Position of dislocation lines in $(1\,\bar{1}\,0)$ glide plane through the 2 nm void equator in crystal C1 at the critical stress at $T = 0$ and 300 K: the latter was obtained for $\dot{\varepsilon} = 10^7$ s^{-1}.

depends on dislocation velocity. For example, if the dislocation approaches the void with a low enough velocity (on starting from a position close to the void or if stress is gradually increased after the dislocation enters the void), it is released from the void at a stress similar to the maximum stress presented in Fig. 7 for the case of constant strain rate application. However, if it starts far

from the void so that it reaches steady state velocity, which depends on the level of applied shear stress (see e.g. [1]), it can pass through the row of voids at a stress significantly lower than τ_c at the same temperature. For example, the penetration process at 100 K occurs for a dislocation moving with $V_d \approx 800$ m/s under $\tau = 60$ MPa in the C1 model. Note that this level of applied stress is less than a third of $\tau_c = 207$ MPa at $T = 0$ K. This effect depends on crystal size, and is related to the kinetic energy stored by the moving dislocation. More detail on this effect will be presented elsewhere. Here we simply emphasise that, in general, the critical stress τ_c *cannot* be obtained in modelling of this type.

4. Results for dislocation–precipitate interaction

4.1. dislocation–precipitate interaction at $T = 0$ K

Examples of stress–strain and ΔE–strain curves obtained for the edge dislocation penetrating a row of bcc Cu precipitates with $D = 2$ nm (339 Cu-atoms) under increasing applied strain in model C1 were presented in Fig. 7 of [3]. The form is similar to the that of Fig. 2, except that for the same D and L the precipitate is a weaker obstacle, with τ_c and maximum ΔE lower than for the void obstacle. The preliminary data in [3] for τ_c for a dislocation to pass through a row of precipitates in the C1 and C2 models have now been obtained across a wide range of D and also extended to C4 model. The values are plotted against D (log scale) in Fig. 9. As with voids (Fig. 4), τ_c depends approximately linearly on the logarithm of D, but with a slope significantly larger than for the same row of voids. The ratio of slopes for different L ($L_1 = 41.4$ nm for C1 and C2 and $L_3 = 61.8$ nm for C4) is about 1.5, which matches the reciprocal of the ratio (L_1/L_3), and is similar to that obtained for voids.

However, the linear fit to $\ln(D)$ is not as good as for voids, and the data suggest different gradients for small and large D. This is because the atomic-level mechanism of interaction between an edge dislocation and a coherent copper precipitate is dependent on the precipitate size. Small precipitates, up to $D = 2$ nm, are sheared by the moving dislocation without any additional effects such as dislocation climb. On passing through such precipitates the dislocation has a critical breaking angle $\varphi > 0$. However, larger precipitates may absorb some point defects, causing the dislocation to climb. Furthermore, due to structural instability of bcc copper, larger precipitates undergo a change associated with a bcc-to-fcc structural transformation. As an example, the projection of four $(1\,\bar{1}\,0)$ atomic planes adjacent to the equator of a 4 nm diameter precipitate (2904 Cu atoms) after dislocation breakaway simulated in model C3 is presented in Fig. 10(a). The overlapping symbols indicate the original two-fold stacking sequence of $\{1\,1\,0\}$ planes in the bcc structure, whereas three regions where symbols are not overlapped describe the fcc phase, i.e. three-fold ABC sequence of $\{1\,1\,1\}$ planes. This transformation provokes absorption of both vacancies and interstitials from the dislocation line, as can be seen in Fig. 10(b), where the shape of the dislocation after it had left the precipitate in Fig. 10(a) is presented in [1 1 1] projection. The line is seen to have climbed in two opposite directions, with the result that 12 vacancies and 6 interstitials were left inside the precipitate, i.e. the net direction of the climb is in the opposite sense to that for void. The influence of the change of mechanism with size is such that for precipitates with $D \geqslant 3$ nm, the shape of the dislocation at τ_c becomes similar to that described

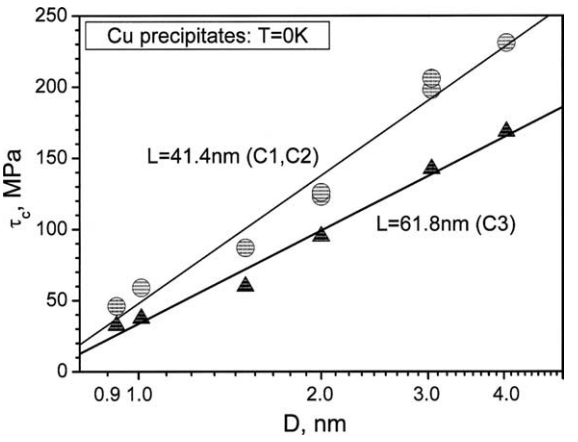

Fig. 9. Dependence of the value of critical resolved shear stress against Cu precipitate diameter: circles are in C1 and C2 and triangles in C3.

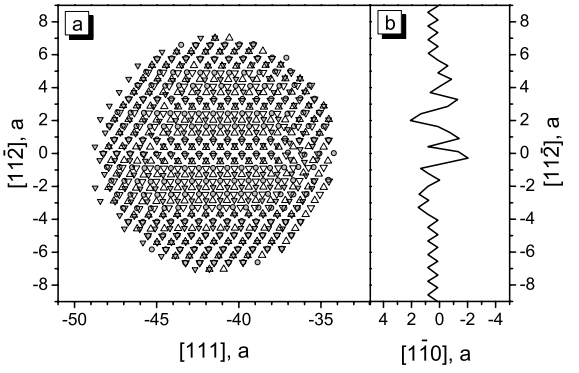

Fig. 10. (a) Position of atoms in four consecutive $(1\,\bar{1}\,0)$ planes through the centre of a 4 nm precipitate after dislocation breakaway at 0 K. (b) [1 1 1] projection of dislocation line after breakaway. Climb to the left side indicates absorption of vacancies whereas that to the right is due to absorption of atoms [3].

for voids in Section 3.1, for the critical leaving angle is essentially zero. Again, however, despite the similarity to the critical shape in the Orowan mechanism for impenetrable obstacles, no Orowan loop is left after the dislocation overcomes a precipitate.

4.2. dislocation–precipitate interaction at $T > 0$ K

As found for voids in Section 3.2, increase of temperature causes a decrease in τ_c for precipitates. The effect can be seen in Fig. 11, where stress–strain curves

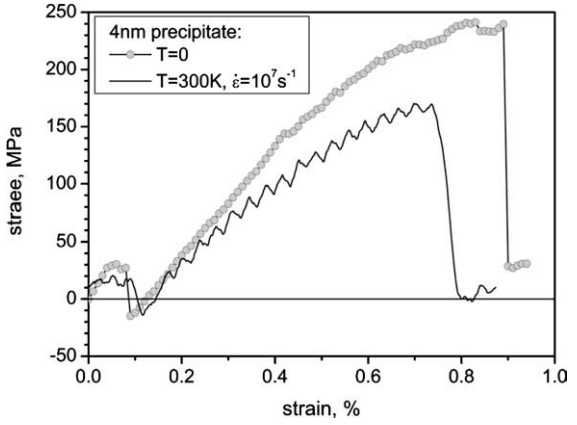

Fig. 11. Applied stress as function of strain in crystal C1 with a 4 nm precipitate at 0 and 300 K ($\dot{\varepsilon} = 10^7$ s^{-1}).

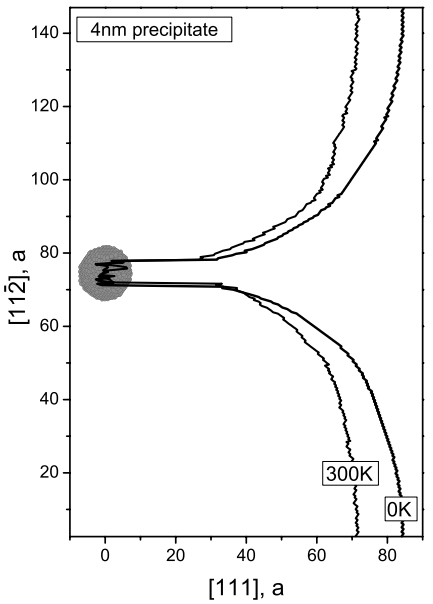

Fig. 12. Dislocation line in the $(1\,\bar{1}\,0)$ slip plane at the critical stress for a 4 nm precipitate in model crystal C1 at 0 and 300 K ($\dot{\varepsilon} = 10^7$ s^{-1}).

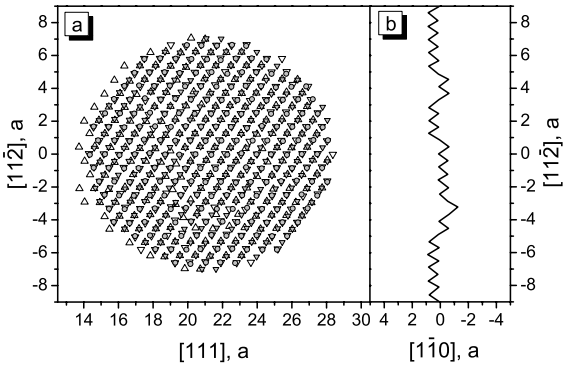

Fig. 13. (a) Position of atoms in four consecutive $(1\,\bar{1}\,0)$ planes through the centre of a 4 nm precipitate after dislocation breakaway at 300 K. (b) [1 1 1] projection of dislocation line after breakaway. Climb to the right is due to absorption of atoms.

obtained for the C2 model with a 4 nm precipitate for either 0 K (static modelling) or 300 K at $\dot{\varepsilon} = 10^7$ s^{-1} (MD) are presented. The decrease of critical stress and strain also affects the dislocation line shape as it leaves the precipitate, as shown in Fig. 12 for the same two cases. Furthermore, we have found that temperature also affects the mechanism of dislocation–precipitate interaction for, in contrast to the static case of Section 4.1 (Fig. 10), the 4 nm precipitate does not show evidence of extensive bcc-to-fcc transformation. This can be seen in Fig. 13 where, as in Fig. 10, the projection of four $(1\,\bar{1}\,0)$ atomic planes (a) and the corresponding dislocation climb shape (b) after the dislocation was released from the precipitate at 300 K and $\dot{\varepsilon} = 10^7$ s^{-1} are shown. Note that at 300 K only vacancies, nine in total, were left inside the precipitate in this case.

5. Discussion

5.1. Mechanisms of dislocation interaction with voids and precipitates

The simulations presented here extend those reported in [3] and provide an extensive data set for void and copper-precipitate strengthening in α-iron at $T = 0$ and $T > 0$ K. The former condition is directly comparable with static simulation based on either line tension or self-stress models in the continuum approximation. We treat this in Sections 5.2 and 5.3. First, we consider the atomic-level mechanisms involved.

The present work confirms the previous finding that strengthening due to small voids and precipitates, $D \leqslant 2$ nm, is significantly different, whereas that for larger obstacles is similar. This is demonstrated, for example, in Fig. 14, where stress–strain dependences simulated in

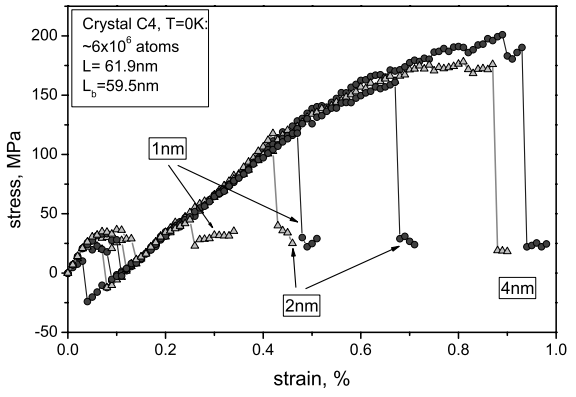

Fig. 14. Applied stress as function of strain in crystal C4 with 1, 2 and 4 nm voids (dark circles) and precipitates (light triangles) at $T = 0$ K.

the C4 model at $T = 0$ K for both voids and precipitates with $D = 1$, 2 and 4 nm are presented. The difference in both the critical stress and strain between the two obstacle types decreases with increasing D and becomes small for $D = 4$ nm. This difference is also reflected in the critical shape of the dislocation line when it leaves the obstacle. Examples for $D = 1$ and 4 nm for the C2 model at $T = 0$ K are presented in Fig. 15. In Fig. 15(a) the dislocation bows-out strongly near the 1nm void, exhibiting an Orowan-like shape with critical angle φ close to zero, whereas it is only slightly bent ($\varphi = 136°$) near the 1nm precipitate, where the simple shear mechanism of the particle operates. In contrast, the two configurations near the 4 nm void and precipitate are similar, as can be seen in Fig. 15(b), where a long ($>20a \sim 6$ nm) dipole consisting of parallel screw segments of opposite sign is formed at τ_c and the breaking angle is essentially zero.

The simulations show that for both voids and precipitates, dislocation climb occurs when the line adopts the shape with $\varphi \approx 0$ at the critical stress. The climb process is not the same for the two types of obstacle, however. The volume of voids is *reduced* due to the line absorbing vacancies and acquiring a superjog, i.e. some atoms are left inside the void surface. Creation of a superjog is an effective mechanism to reduce the critical resolved shear stress, for, as discussed in [3], there is a drop of several % in stress just before breakaway occurs. This mechanism seems to occur more easily than mutual annihilation of the two screw segments by glide, presumably due to the high Peierls stress associated with the non-planar core structure of screw dislocations in the bcc metals. In contrast to void shrinkage, the effective size of precipitates *increases*, for the number of vacancies absorbed is larger than that of Cu interstitials created (in the configuration of $\langle 1\,1\,1\rangle$ crowdions) inside a precipitate with $D > 2$ nm (see e.g. Fig. 10). Again, however, as with voids, defect formation inside the precipitate and dislocation climb are associated with a drop in τ, just as the line breaks away [3].

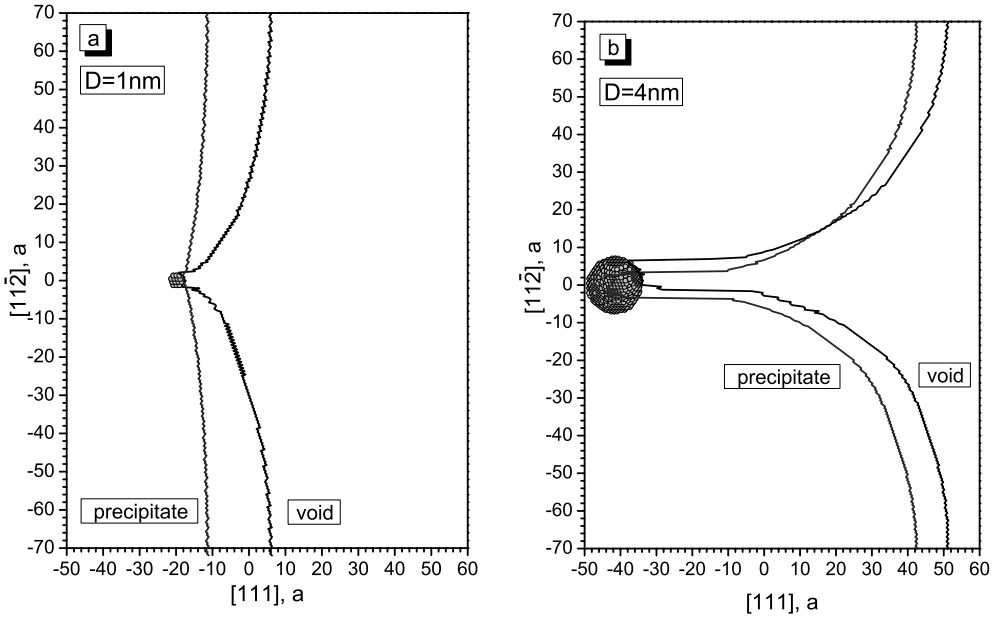

Fig. 15. Dislocation line in the $(1\,\bar{1}\,0)$ slip plane at the critical stress for (a) 1 nm obstacles and (b) 4 nm obstacles in model crystal C2 at $T = 0$ K (from [3]).

5.2. Comparison with the Orowan mechanism for dislocation–obstacle interaction

The τ_c values for void and precipitate strengthening are compared in Fig. 16, where the critical shear stress, in units of Gb/L is plotted against the harmonic mean of obstacle spacing and diameter $(D^{-1}+L^{-1})^{-1}$, in units of b. The value of G has been taken as 62.5 GPa, which is the effective isotropic shear modulus estimated using anisotropic elasticity for a dislocation of the $\langle 1\,1\,1\rangle\{1\,1\,\bar{1}\,0\}$ glide system in Fe [7]. The harmonic mean has been chosen because such a plot was found to give an excellent correlation for the Orowan stress of a row of impenetrable obstacles in a computer simulation based on elasticity theory in which the self-stress of a flexible dislocation was included explicitly [8]. The rationale for this is that the harmonic mean tends to D when $D \ll L$ and L when $L \ll D$, in recognition that the critical breakaway line configuration of the Orowan process is achieved when the applied stress can draw out a dipole of spacing D (energy $\propto \ln(D)$) when $D \ll L$ and spacing L (energy $\propto \ln(L)$) when $L \ll D$. The dashed line in Fig. 16 is the fit obtained in [8] when r_0, the dislocation core cutoff radius used as a unit of length for D and L, is set equal to b.

The continuum model of a flexible dislocation in [8] was developed further by Scattergood and Bacon in [9] to simulate a dislocation passing through a row of voids in an anisotropic medium. The boundary condition for a dislocation at a void surface was treated as though the terminating segment is in equilibrium at a flat, infinite surface, with a point force tangential to the surface at the termination included to represent the effect of creation of a surface step. A range of surface energy values, γ, was considered and the solid line in Fig. 16 is for the highest value thought reasonable: $\gamma = 3(Gb/4\pi)\ln(R/r_0)$, where R is the outer cutoff radius in the energy of dislocation. Like r_0, R is an unavoidable arbitrary parameter arising from the use of elasticity theory. Again, we have used $r_0 = b$. The lines obtained in [8,9] from the continuum simulation with self-stress included are represented by the equation:

$$\tau_c = \frac{Gb}{2\pi L}\left[\ln(D^{-1}+L^{-1})^{-1} + B\right], \tag{2}$$

where $B = 0.7$ for impenetrable obstacles and 1.52 for voids. The void data obtained in the present atomic-level modelling are seen from Fig. 16 to fit the same relationship well, despite the fact the continuum treatments contained several approximations and were not envisaged to apply to very small obstacles. (The smallest D considered in [9] was $10r_0$, which is about 2.5 nm if $r_0 = b$.) The agreement stems from the observation that the dislocation segments that emerge from a void at the critical stress are almost parallel, thereby matching the conditions for the Orowan stress. They are screw in character, so the shear stress acting over the length L draws out a screw dipole of spacing D, which has a line tension proportional to $\ln(D)$. The data in Fig. 16 for the smallest void does not fit this model quite so well, probably because the angle φ in the critical condition is greater than zero.

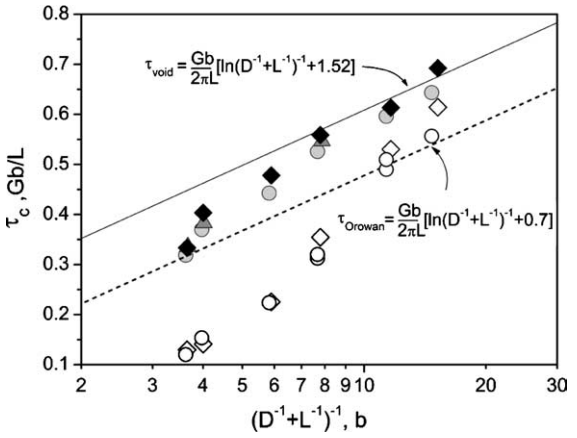

Fig. 16. Critical resolved shear stress τ_c (units Gb/L) versus the harmonic mean of obstacle spacing, L, and diameter, D, (units b) for voids (full symbols) and precipitates (hollow symbols): circles in crystals C1 and C2, diamonds in C4 and triangles in C3. Lines show empirical correlations found by continuum simulation for voids (solid line) and for impenetrable obstacles via the Orowan mechanism [9] (dashed line).

A notable feature of the data in Fig. 16 is that the τ_c values for the smaller copper precipitates fall well below the condition found for the Orowan and void-strengthening process. It is explained in Section 4 that such obstacles are sheared by dislocations with critical breaking angle $\varphi > 0$. This is shown clearly by the critical line shapes for precipitates of different size in the C1 crystal in Fig. 17, where φ decreases from 145° to 0° as D increases from 0.9 to 3 nm. Hence, the correlation based on $\varphi = 0°$ expressed by Eq. (2) cannot be expected to apply to small precipitates. For large ones, however, when the line becomes jogged and the particle is large enough for the dislocation to induce a phase change in the unstable bcc copper, τ_c approaches the value for voids of the same size and the correlation of Eq. (2) appears to apply. The possible importance of the bcc-to-fcc transformation as a strengthening mechanism was first recognised in the atomic-scale study of the interaction energy of a screw dislocation with a Cu precipitate in iron at $T = 0$ K by Harry and Bacon [10] (see next section).

5.3. Comparison with line tension models of obstacle strengthening

A crucial aspect to the good fit between the critical stress obtained here by atomic scale simulations and the

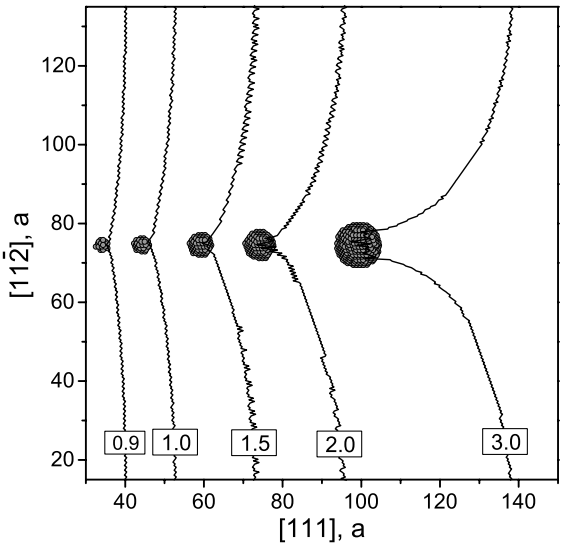

Fig. 17. Dislocation line in the $(1\,\bar{1}\,0)$ slip plane at the critical stress for Cu precipitates of different size. Diameter is indicated in each case. Larger precipitates have zero critical angle [3].

correlations for Orowan and void strengthening deduced in [8,9] from the continuum treatment is the fact that dislocation self-stress effects were included in the elastic modelling, i.e. the line tension approximation was not used. Self-interaction between the two line segments that are drawn out parallel ($\varphi = 0$) for strong obstacles controls the critical stress at which this configuration is realised. This effect is not described in the line tension approximation.

In this approximation, self-interaction is neglected and self-stress arises only from local curvature. The strength by which an obstacle resists dislocation motion is then defined solely by the critical value of the cusp angle between line segments that meet at the obstacle (e.g. see Chapter 10 of Hull and Bacon [6]). Unfortunately, the critical value of φ required for line-tension based calculations of τ_c for a given type of obstacle is not known a priori. This can be illustrated by considering the model of Russell and Brown [11], which has been used frequently to estimate the value of τ_c for precipitates of Cu in Fe. It is based on constant line tension approximation and the premise that the precipitates have a lower elastic modulus than the matrix, i.e. the dislocation energy per unit length in Cu, E_{prpt}, is less than that in Fe, E_{matrix}. This modulus hardening model gives for a row of precipitates of spacing L:

$$\tau_c = \frac{Gb}{L}\left[\cos\left(\frac{\varphi}{2}\right)\right] = \frac{Gb}{L}\left[1 - \frac{E_{\mathrm{prpt}}}{E_{\mathrm{matrix}}}\right]^{1/2}, \quad \text{if } \frac{\varphi}{2} = \sin^{-1}\frac{E_{\mathrm{prpt}}}{E_{\mathrm{matrix}}} \leqslant 50^\circ, \tag{3a}$$

$$\tau_c = \frac{Gb}{L}\left[\cos\left(\frac{\varphi}{2}\right)\right]^{3/2} = \frac{Gb}{L}\left[1 - \frac{E_{\mathrm{prpt}}}{E_{\mathrm{matrix}}}\right]^{3/4}, \quad \text{if } \frac{\varphi}{2} = \sin^{-1}\frac{E_{\mathrm{prpt}}}{E_{\mathrm{matrix}}} \geqslant 50^\circ. \tag{3b}$$

Although ΔE does change sign as the line enters a precipitate (see Fig. 7 of [3]), as it does for a void (region II of Fig. 2), it is not possible to determine E_{prpt} for such small, unstable particles. If we were to assume that the critical angle when a dislocation breaks from a precipitate of diameter of up to 3 nm in the line tension treatment can be determined from the critical shapes in Fig. 17, then, as shown in Fig. 18, the results obtained from Eqs. (3a) and (3b) overestimate the strengthening significantly. This is because the Russell–Brown model assumes constant line tension and neglects the important self-interactions between the two dislocation branches that emerge from a precipitate, e.g. when $\varphi = 0$, Eq. (3a) gives a much higher τ_c than Eq. (1).

Note, however, that when $E_{\mathrm{prpt}} = 0$, i.e. a void, the Russell–Brown model *does* correctly predict $\varphi = 0$, the Orowan condition, albeit with an imprecise stress. More generally, if τ_c in Eq. (3a) for strong obstacles is set equal to the accurate value given by Eq. (2), the critical line-tension angle is given by

$$\cos\left(\frac{\phi}{2}\right) = \frac{1}{2\pi}[\ln(D^{-1} + L^{-1})^{-1} + B]. \tag{4}$$

For voids ($B = 1.52$) with the size and spacing values studied here, φ from Eq. (3) lies in the range ~90–110°, rather than close to zero as found in the present simulations and those in [8,9]. In other words, self-interactions reduce τ_c to values it would have if voids and large Cu precipitates were *weak* obstacles in the line tension

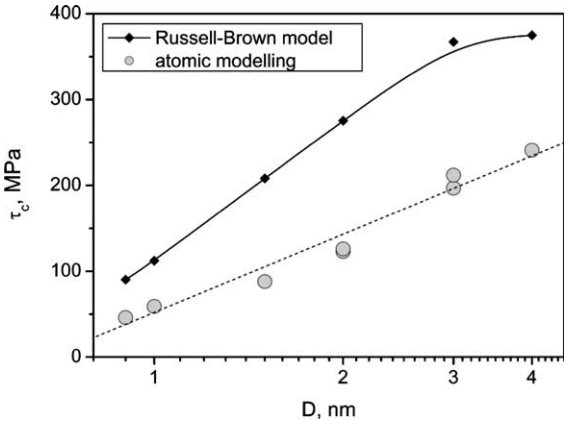

Fig. 18. Comparison of τ_c obtained by atomic modelling (grey circles) and the Russell–Brown model (Eq. (3)) using the critical angles from simulation (full diamonds) [3].

model (This is why the Russell–Brown formula with the true angles overestimates the strength (Fig. 18).). This conclusion was first discussed for Orowan strengthening in [8]. It does not mean that such obstacles can be treated in the line-tension framework by simply choosing a large φ for breakaway, because then the shape of the bowing line would be in error, and this would affect the statistics of dislocation–obstacle interaction in a realistic random array of obstacles. Hence, care has to be exercised in selecting the parameters to define obstacle strength in modelling based on the continuum approximation.

5.4. Temperature, stress and strain rate effects

The results of Sections 3.2 and 4.2 show that temperature affects the interaction of an edge dislocation with voids and coherent precipitates by reducing τ_c: at 300 K it falls to ~25% of its value at $T = 0$ K. The mechanism of this reduction is not yet fully understood. The first, and most obvious, contribution is related to the increased mobility of a screw dislocation at high temperature. This affects the final stage of the dislocation–obstacle interaction when τ_c is governed by the interaction between two parallel screw segments: at non-zero T the Peierls stress decreases and this assists the mutual annihilation of these segments. The significance of this effect should increase for larger obstacles. Other effects for both voids and precipitates may arise from the thermally-assisted motion of dislocation over the void surface or the precipitate-matrix interface, and form defect/superjog formation. Finally, for the copper precipitates, the role of temperature in the phase transformation may have an effect. An unexpected result of the present work is that the bcc-to-fcc transformation inside the 4 nm precipitate was suppressed at 300 K. A factor here may be that the precipitates were modelled as 100% Cu without vacancies inside. It is known that a vacancy population enhances precipitate transformation [12,13] and without it temperature assists a dislocation to create more vacancies, as observed here for the 4nm precipitate. To study this effect further, simulation of the interaction between a dislocation and precipitates containing vacancies is now in progress.

Temperature effects also interact with stress and strain rate effects. For example, on reaching its steady state velocity at $\tau = 60$ MPa in crystal C1, the dislocation was found to pass through the 2 nm void at 100 K but was unable to do so at 300 K. The reason is that due to the temperature dependence of the drag coefficient, the steady state velocity for 60 MPa reduces from ~800 m/s at 100 K to ~600 m/s at 300 K. This reduces the kinetic energy of the moving dislocation, thereby making penetration through the 2 nm void impossible. More detail on kinetic effects in dislocation–obstacle interactions will be published elsewhere [14]. When strain is applied in dynamic simulations, temperature effects depend on the applied strain rate $\dot{\varepsilon}$ because the process of dislocation–obstacle interaction becomes closer to equilibrium as $\dot{\varepsilon}$ decreases. For the strain rates we have considered, i.e. 2×10^6–10^8 s^{-1}, the corresponding steady-state dislocation velocities at 100 and 300 K are from ~5 to ~240 m/s, and there is a decrease in τ_c for void obstacles at lower velocity without a noticeable difference in interaction mechanism. This work is in progress [14]. It seems likely that the effect will be different for a coherent Cu precipitate containing a concentration of vacancies, for the bcc-to-fcc transformation rate, and corresponding transformation strengthening, should be dependent on $\dot{\varepsilon}$ and T.

5.5. Comments on linking atomic to continuum dislocation dynamics simulations

As emphasised in Section 1 modelling of mechanical properties requires a multiscale approach. It is anticipated that the details of the characteristic parameters of dislocation–obstacle interaction obtained in atomic-level modelling by MD will have to be incorporated in large-scale dislocation dynamics (DD) simulations based on the continuum approximation. Such parameters include the maximum obstacle force, critical breaking angle, Peierls stress, etc. (As noted earlier, non-dynamic continuum modelling can be compared directly with the static ($T = 0$ K) atomic-scale results because they avoid assumptions about thermally activated processes.) The results described here reveal how detailed the atomic-scale studies have to be if they are to provide both qualitative and quantitative pictures, because the atomic mechanisms control the obstacle size range over which any one set of parameters apply and are almost impossible to predict. Thus, voids appear as strong obstacles with small critical breaking angle φ, whereas Cu precipitates are weak obstacles when small, e.g. they are overcome with large φ, and become strong obstacles as they grow. This transition arises from a transformation on the atomic scale. Furthermore, dislocation climb is associated with breakaway from both voids and the larger precipitates, and again the underlying processes (of point defect creation and absorption) are atomic in nature.

A recognised weakness of DD simulations is that they require the use of an arbitrary length parameter r_0 (and occasionally of an outer cutoff R in addition). The absolute value of this probably depends not only on the material but also on the form of the line, e.g. straight or curved. Another valuable use of MD simulation is that when the results can be compared directly with those of DD modelling of the same phenomenon, r_0 can be estimated. It is shown above that the choice $r_0 = b$ provides a good correspondence between the present MD data and the earlier studies [8,9]. However, in other situations, a different value may apply, e.g. a comparison of energy calculated by elasticity theory and MD

suggests that $r_0 \approx 3b$ for the straight edge dislocation in iron [15].

It should be noted that the empirical analytic expression (Eq. (2)) for strengthening due to voids and precipitates obtained by MD is for a linear row of obstacles of equal size and spacing. Real obstacles are usually in random, three-dimensional arrays with a distribution of size and spacing. MD is unlikely to achieve the scale required to simulate this in the near future, whereas DD modelling can do it now. The usefulness of the results for a linear row has been demonstrated in [16] for the case of incoherent precipitates.

As far as stress and strain rate effects at non-zero temperature are concerned, they cannot be included directly in continuum DD modelling at the moment. Appropriate description have to be developed; e.g. for dislocation motion over the void and precipitate surface and formation of surface steps, defect absorption and kinetic effects in dislocation–obstacle interaction. Approximations have to be made and the difficulty lies in parameterisation, e.g. choice of characteristic energy or/and time, of the controlling mechanisms, which requires design of the corresponding continuum models. A separate problem arises in treatment of temperature-dependent mechanisms of dislocation–obstacle interactions. Thus it was demonstrated here that at $T = 0$ K a dislocation penetrates through voids and large precipitates to an Orowan-like shape, i.e. the critical stress is controlled by self-interaction of the dislocation as it bows out between the obstacles. This changes at $T > 0$ K when temperature enhances (a) self-interaction by reducing the critical stress for dislocation motion, (b) motion of the dislocation over obstacle-matrix interface, (c) absorption of defects by the dislocation line, i.e. climb, and (d) structural transformation inside solid obstacles, e.g. coherent precipitates.

6. Conclusions

1. The process by which an edge dislocation cuts a linear row of spherical voids or coherent copper precipitates with diameter, D, up to 4 nm and spacing, L, up to 83 nm in α-iron at zero and non-zero temperature has been studied by atomic-scale modelling. The applied stress required, the dislocation line shape, the atomic mechanisms and the effects of temperature, T, and applied strain rate have been determined.
2. Voids are strong obstacles, for which the dislocation breaking angle $\varphi = 0$ at the critical stress, τ_c, even for diameter down to 1 nm. The critical line shape is qualitatively similar to that for the Orowan mechanism, i.e. a screw dipole is drawn out at τ_c, when the dislocation breaks from the void. The dipole is stabilised by the high Peierls stress of the screw dislocation in iron at $T = 0$ K.
3. A dislocation always climbs by absorbing vacancies and reducing the void size as it breaks away from the void. Climb is associated with a small reduction in τ_c.
4. The mechanism by which a dislocation passes through a coherent Cu precipitate depends on the precipitate size. For small precipitates, $D \leqslant 2$ nm, a simple shear displacement mechanism occurs and the critical breaking angle φ is >0. No climb or precipitate transformation arises with this mechanism. On passing through larger precipitates, a dislocation leaves point defects, both vacancies and interstitials, thereby climbing and provoking a phase transformation towards the stable fcc structure of Cu. This mechanism results in a strong obstacle and the critical line shape is again qualitatively similar to the Orowan configuration ($\varphi = 0$), but Orowan loops are not left around the precipitate.
5. Effects due to temperature, strain rate and stress are observed in dynamics modelling. In general, τ_c decreases at high temperature, low strain rate (strain applied) and high dislocation velocity (stress applied). An understanding of these effects is necessary for creation of realistic large-scale (continuum) dislocation dynamics models.
6. A comparison has been made of τ_c and φ obtained in the present work for $T = 0$ K with values found in earlier modelling of Orowan and void strengthening using the continuum approximation [8,9]. This validates the empirical relationship (Eq. (2)) between τ_c and D and L obtained in the previous studies, and determines the arbitrary dislocation core cutoff radius, r_0, in the continuum treatment to be equal to b.
7. Comparison of τ_c with values given by the line tension treatment of obstacle strengthening shows that although the actual critical breaking angle of the dislocation is close to zero for voids and large precipitates, breakaway occurs at a stress where φ would be much greater than zero in the line tension approximation. This emphasises the importance of dislocation self-interaction in the real situation.
8. The role of atomic-scale simulation in obtaining parameters and insight for mechanisms required for continuum-scale dislocation dynamics modelling of strengthening processes has been discussed. Different atomic-scale simulation methods, i.e. static ($T = 0$ K) and dynamic ($T > 0$ K), have their own limitations and advantages, and should be used to investigate different aspects of dislocation–obstacle interaction.

Acknowledgements

The authors acknowledge stimulating discussions with Professor P. Gumbsch and Dr V. Mohles. This research was supported by the UK Engineering and

Physical Sciences Research Council and a JREI grant from Higher Education Funding Council for England.

References

[1] Yu.N. Osetsky, D.J. Bacon, Modell. Simul. Mater. Sci. Eng. 11 (2003) 427.
[2] M.I. Baskes, M.S. Daw, in: N. Moody, A. Thompson (Eds.), Fourth International Conference on the Effects of Hydrogen on the Behaviour of Materials (Jackson Lake Lodge, Moran, WY), The Minerals, Metals and Materials Society, Warrendale, PA, 1989.
[3] Yu.N. Osetsky, D.J. Bacon, V. Mohles, Philos. Mag., in press.
[4] G.J. Ackland, D.J. Bacon, A.F. Calder, T. Harry, Philos. Mag. A 75 (1997) 713.
[5] A.J. Ackland, G. Tichy, V. Vitek, M.V. Finnis, Philos. Mag. A 56 (1987) 735.
[6] D. Hull, D.J. Bacon, Introduction to Dislocations, 4th Ed., Butterworth-Heinemann, Oxford, 2001.
[7] D.J. Bacon, in: B.A. Bilby, K.J. Miller, J.R. Willis (Eds.), Fundamentals of Deformation and Fracture, Cambridge University, 1985, p. 401.
[8] D.J. Bacon, U.F. Kocks, R.O. Scattergood, Philos. Mag. 28 (1973) 1241.
[9] R.O. Scattergood, D.J. Bacon, Acta Metall. 30 (1982) 1665.
[10] T. Harry, D.J. Bacon, Acta Mater. 50 (2002) 195;
T. Harry, D.J. Bacon, Acta Mater. 50 (2002) 209.
[11] K.C. Russell, L.M. Brown, Acta. Metall. 20 (1972) 969.
[12] Yu.N. Osetsky, A. Serra, Philos. Mag. A 75 (1997) 1097.
[13] J.J. Balckstock, G. Ackland, Philos. Mag. A 81 (2001) 2127.
[14] Yu.N. Osetsky, D.J. Bacon, in: H. Kitagawa, Y. Shibutani (Eds.), 'IUTAM Symp. on Mesoscopic Dynamics of Fracture Process and Materials Strength', Kluwer Academic, 2003, in press.
[15] Yu.N. Osetsky, D.J. Bacon, F. Gao, A. Serra, B.N. Singh, J. Nucl. Mater. 283–287 (2000) 784.
[16] V. Mohles, E. Nembach, Acta Mater. 49 (2001) 2405.